

# Experimental study on shear capacity of circular concrete filled steel tubes

Congzhen Xiao, Shaohuai Cai, Tao Chen\* and Chunli Xu

*China Academy of Building Research, No. 30 Beisanhuandonglu, Chaoyang District, Beijing, China*

*(Received April 10, 2012, Revised August 06, 2012, Accepted August 15, 2012)*

**Abstract.** Concrete filled steel tube (CFST) structures have recently seen wide use in China, but studies of the shear problem of CFST are inadequate. This paper presents an experimental study on the shear capacity of circular concrete filled steel tube (CCFT) specimens with and without axial compression force. Shear capacity, ductility, and damage modes of CCFTs were investigated and compared. Test results revealed the following: 1) CCFTs with a small shear span ratio may fail in shear in a ductile manner; 2) Several factors including section size, material properties, shear span ratio, axial compression ratio, and confinement index affect the shear capacity of CCFTs. Based on test results and analysis, this paper proposes a design formula for the shear capacity of CCFTs.

**Keywords:** CFST; CCFT; shear capacity; shear span ratio; axial compression ratio; confinement index.

---

## 1. Introduction

In recent decades, CFST structures have been widely used in China. CFST structures are efficient in construction, combining the advantages of steel and concrete: delayed local buckling of the steel tube outside, increased strength of the concrete inside due to the confinement effect, less drying shrinkage and creep as compared to normal concrete (e.g., Morino *et al.* 2001). CCFTs can provide better confinement, greater shear reinforcement to the concrete inside, and better composite interaction between the two materials than rectangular CFSTs (e.g., Roeder *et al.* 1999, 2009). This paper focuses primarily on CCFTs.

Compression, bending, shear, and torsion are critical characteristics for structure members. Many studies of CCFTs have focused on compression, bending (e.g., Tomii *et al.* 1977, Goode *et al.* 2008, Roeder *et al.* 2010), and torsion (e.g., Han *et al.* 2007, Lee *et al.* 2009), but few studies have focused on the shear problem.

According to past engineering practices, most CCFTs in construction have heights more than three times their diameters, the carrying capacity of the CCFTs is generally controlled by the effect of axial compression or bending, and the horizontal shear problem is neither prominent nor influential on design. Therefore, previous systematic studies for the shear problem of CCFTs are inadequate.

ACI 318 (2008), Eurocode 4 (2007), and the present Chinese Code ("Steel concrete structure design

---

\* Corresponding author, Mr., E-mail: [chentao@cabrtech.com](mailto:chentao@cabrtech.com)

and construction procedures (CECS 28:90)”) do not have any provisions for the shear problem of CCFTs. AISC 360-10 (2010) offers a superposition method to determine the shear strength of CCFTs in Chapter I4, but the method is relatively simple and unrefined. Yang *et al.* (1992), and Han *et al.* (1994), using steel and concrete of CFST as composite materials, analyzed the shear strength, and proposed formulas for calculation, but without considering that the shear strength of CFST is tied to axial force.

With the continued development of engineering practices, the shear problem is becoming conspicuous in the design of small shear span CCFTs and some other cases such as CCFT columns with diagonal bracing between nodes, column joints and heavy beams with large spans and so on. To solve this problem, special experimental studies were carried out in the structure lab of the China Academy of Building Research.

## 2. Experiment

### 2.1 Test specimens

In addition to the geometry section and material strength properties, shear span ratio ( $a/D$  in Fig. 1(b)) and axial compression ratio (axial compression force/axial compression bearing capacity) may affect the shear capacity of CCFTs. Two batches of 58 specimens with different shear span ratios (0.14, 0.4, 0.5, and 1.0) and axial compression ratios (0, 0.2 and 0.4) were studied. The various steel tubes specifications and concrete strengths are shown in Table 1 and Table 2.

First, the empty steel tube was cut to the required length, and an endplate (a square steel plate of 190 mm × 190 mm × 10 mm) was welded to one end of the tube. The endplate and the tube had the same geometric centre. Second, the specimen was set up with the endplate at the bottom, and concrete was poured into the tube vibrating with plug-in vibrators. Then, the concrete surface at the top of the tube was carefully smoothed. After 14 days, the concrete surface was smoothed again with a high-strength cement mortar. Finally, the other endplate was welded to the top of the tube.

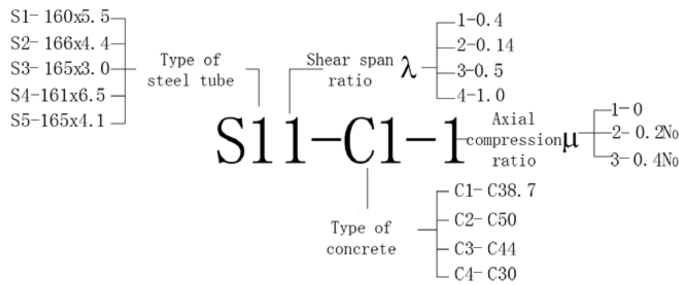
Naming rules for specimens are as follows

Table 1 Steel tubes specifications

Type	Dimension [mm]	Yield strength $f_s$ [MPa]	Ultimate tensile strength $f_u$ [MPa]
S1	160 × 5.5	377	442
S2	166 × 4.4	345	427
S3	165 × 3.0	408	487
S4	161 × 6.5	445	550
S5	165 × 4.1	385	482

Table 2 Concrete strengths

Type	C1	C2	C3	C4
Cubic compressive strength $f_{cu}$ [MPa]	38.7	50.0	44.0	30.0
Axial compressive strength $f_c$ [MPa]	25.9	32.4	29.5	20.1



2.2 Test setup and test procedure

Fig. 1 shows the test setup and loading plan. The specimen was put on two supports. Axial compression load ( $N$ ) was applied with a self-balancing reaction frame, and shear force was achieved by lateral load ( $P$ ) applied in the middle of the specimen.

Strains at critical locations of tube and loading forces were measured by sensors. The deflection in the middle of specimen was measured by displacement gauge.

For specimens without axial compression load, lateral load was applied step by step. For specimens with axial compression ratio of 0.2 and 0.4, axial compression load was increased to a predetermined value and remained constant during the test, then lateral load was applied. In the elastic stage of the specimen, the lateral load step was about 1/10 of estimated ultimate load. When the specimen was close to yield, lateral load step was reduced. The duration of each load stage was about 2 minutes, with loading speed reduced when the specimen was close to failure.

Failure was defined as the sudden loss of load carrying capacity; rupture of the steel; onset of buckling or severe deformation; load carrying capacity loss at 15% of the ultimate load.

3. Test results

3.1 Failure mode

In the early stage of lateral loading, deflection of the specimen and changes in the overall shape was

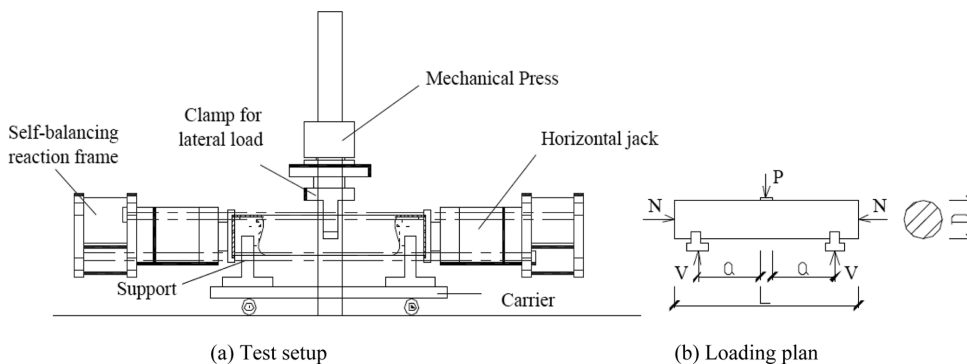


Fig. 1 Test setup and loading plan

not prominent. The specimen was mainly in elastic stage. With the increase of lateral load, the tube buckled at the action place of lateral load. Then the specimen failed due to sharp increase in deflection.

Two types of failure modes were observed during the test.

### 3.1.1. Shear dominated failure

Specimens with a shear span ratio of 0.14 and 0.4 had the same failure mode: great shear deformation occurred between lateral load and the supports, and the surface oxide layer was peeled off. Some specimens were even sheared open (Figs. 2 and 3). In the case of specimens sheared open at the supports, the concrete inside was crushed and flowed out in powder form. For specimens not sheared open at the supports, the steel tube was cut open after the test. It was found that the concrete inside was

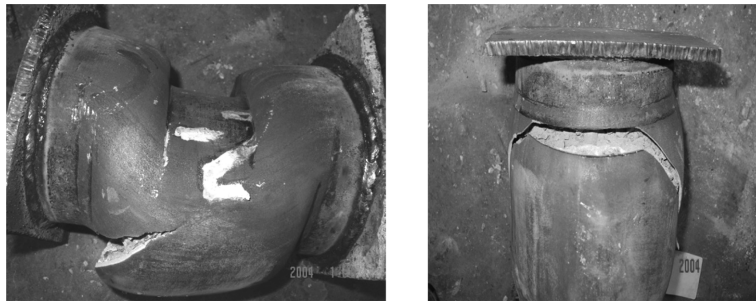
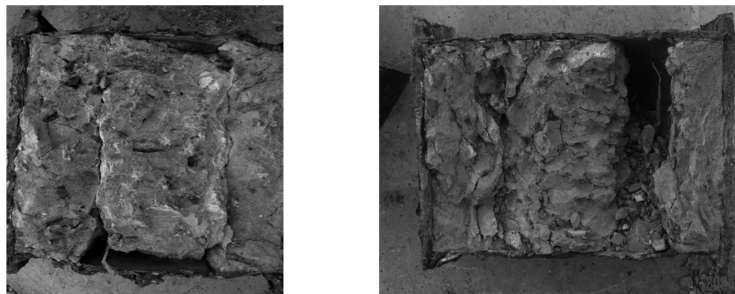


Fig. 2 Failure mode of specimens sheared open



Fig. 3 Failure mode of specimens not sheared open



(a) Specimens with small shear span ratio (b) Specimens with large shear span ratio

Fig. 4 Concrete of specimens not sheared open

not separated from steel tube outside, but contained thin and irregular cracks. Specimens with a small shear span ratio (0.14) had a failure mode indicating direct shear failure and the region of concrete failure was small. Specimens with a large shear span ratio (0.4) had a failure mode indicating diagonal compression failure, and the concrete sustained diagonal cracks (Fig. 4).

### 3.1.2. Bending dominated failure

Specimens with a shear span ratio of 0.5 and 1.0 suffered bending failure mode: steel tube ruptured in the tension zone (Fig. 5). The steel tube was cut open after the test, and it was discovered that the tension zone of the concrete suffered uniform and dense transverse cracks, with crack depth reaching more than half of the section height; also, some of the concrete in the tension zone extruded along with the steel tube.

Specimens with a shear span ratio of 0.5 showed both bending failure and shear failure.

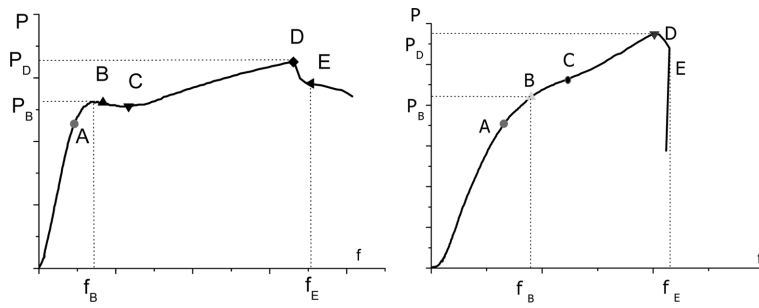
### 3.2 Load-displacement curve and shear capacity

The load-displacement curves ( $P$ - $f$  curve) measured can be divided into two types by shape characteristics: one type of curve has a peak point in the yielding stage, as shown in Fig. 6(a) (Point B);



(a) Specimens with shear span ratio of 1.0 (b) Specimens with shear span ratio of 0.5

Fig. 5 Bending dominated failure



(a) Curve with peak at point B (b) Curve with inflection at point B

Fig. 6 Two types of  $P$ - $f$  curves

the other type of curve has no peak point in the yielding stage but an inflection point where the slope of the curve changes rapidly, as shown in Fig. 6(b) (Point B).

The load ( $P_B$ ) corresponding to the peak point or inflection point can be referred to as ultimate load, and the shear force corresponding to  $P_B$  can be referred to as shear capacity. In this test,  $V_u = P_B/2$ .

In the  $P$ - $f$  curve, the OA segment is linear and shows the specimen is working in the elastic stage; the ABC segment is concave and shows the specimen is working in the elastic-plastic stage; and the CD segment is convex and shows the specimen is working in the strengthening stage. In the strengthening stage, the larger the shear span ratio ( $\lambda$ ) or axial compression ratio ( $\mu$ ) of a specimen is, the sharper the slope of the curve behaves. Point D in the  $P$ - $f$  curve shows the specimen reached maximum capacity. Point E, referred to as the point of failure, shows the capacity drops down to 85% of maximum capacity.

Most of the specimens with a small shear span ratio and axial compression had no peak points B in their  $P$ - $f$  curves, and specimens with a higher shear span ratio and axial compression generally had peak points B. It was difficult to determine inflection B, and so point B on the  $P$ - $f$  curve is indicated at the intersection point of the tangents of segment OA and CD.

Table 3 shows the test results of  $P_B$ ,  $P_D$ ,  $f_B$ , and  $f_E$ . Ductility factor is defined by  $f_E/f_B$ .  $\theta$  is confinement

Table 3 Main parameters and test results

Name	Dimension D×L×t [mm]	$\theta$	$\lambda$	$N$ [kN]	$P_B$ [kN]	$f_B$ [mm]	$P_D$ [kN]	$f_E$ [mm]	Ductility factor
S11-C1-1	160×238×5.5	2.17	0.4	0	1250	11.1	1962	46.2	4.16
S11-C2-1	160×238×5.5	1.93	0.4	0	1350	11.0	1881	44.2	4.02
S11-C3-1	160×238×5.5	2.12	0.4	0	1300	9.4	1859	43.4	4.62
S21-C1-1	166×238×4.4	1.38	0.4	0	1030	7.8	1501	42.7	5.47
S21-C2-1	166×238×4.4	1.23	0.4	0	1135	7.1	1550	38.3	5.39
S21-C3-1	166×238×4.4	1.35	0.4	0	1050	5.1	1491	36.9	7.24
S31-C1-1	165×238×3	1.01	0.4	0	750	7.4	1019	36.0	4.86
S31-C2-1	165×238×3	0.90	0.4	0	830	7.0	1095	34.2	4.89
S31-C3-1	165×238×3	0.99	0.4	0	770	6.6	1051	33.5	5.08
S11-C1-2	160×238×5.5	2.17	0.4	466	1455	11.0	2027	41.7	3.79
S11-C2-2	160×238×5.5	1.93	0.4	487	1500	8.5	1935	43.4	5.11
S11-C3-2	160×238×5.5	2.12	0.4	470	1560	11.7	2043	38.5	3.29
S21-C1-2	166×238×4.4	1.38	0.4	397	1260	8.4	1734	40.6	4.83
S21-C2-2	166×238×4.4	1.23	0.4	419	1306	7.6	1626	40.0	5.26
S21-C3-2	166×238×4.4	1.35	0.4	401	1350	8.0	1691	30.5	3.81
S31-C1-2	165×238×3	1.01	0.4	342	960	6.7	1257	34.3	5.12
S31-C2-2	165×238×3	0.90	0.4	356	970	9.5	1182	31.9	3.36
S31-C3-2	165×238×3	0.99	0.4	344	990	4.3	1182	27.5	6.40
S11-C1-3	160×238×5.5	2.17	0.4	933	1404	6.4	1762	20.9	3.27
S11-C2-3	160×238×5.5	1.93	0.4	975	1620	3.8	2081	23.2	6.11
S21-C1-3	166×238×4.4	1.38	0.4	795	1300	6.3	1637	23.0	3.65
S21-C2-3	166×238×4.4	1.23	0.4	838	1400	9.1	1816	33.8	3.71
S31-C1-3	165×238×3	1.01	0.4	684	1090	5.6	1285	23.9	4.27
S31-C2-3	165×238×3	0.90	0.4	711	1160	4.6	1360	23.0	5.00

Table 3 Main parameters and test results (Continued)

Name	Dimension D×L×t [mm]	$\theta$	$\lambda$	$N$ [kN]	$P_B$ [kN]	$f_B$ [mm]	$P_D$ [kN]	$f_E$ [mm]	Ductility factor
S12-C1-1	160×154×5.5	2.17	0.14	0	1000	4.5	1512	17.5	3.89
S12-C2-1	160×154×5.5	1.93	0.14	0	1050	5.0	1547	26.4	5.28
S12-C3-1	160×154×5.5	2.12	0.14	0	1100	6.1	1507	27.3	4.48
Long to short S12-C3-1	160×238×5.5	2.12	0.14	0	1400	7.9	2569	24.1	3.05
Long to short S22-C3-1	166×238×4.4	1.35	0.14	0	1300	5.9	2005	23.6	4.00
Long to short S32-C3-1	165×238×3	0.99	0.14	0	900	5.2	1382	20.2	3.88
S22-C1-1	166×154×4.4	1.38	0.14	0	1050	5.9	1957	31.7	5.37
S22-C2-1	166×154×4.4	1.23	0.14	0	1150	6.5	1957	33.8	5.20
S22-C3-1	166×154×4.4	1.35	0.14	0	1125	6.2	1886	26.8	4.32
S32-C1-1	165×154×3	1.01	0.14	0	800	5.4	1371	27.0	5.00
S32-C2-1	165×154×3	0.90	0.14	0	850	3.9	1393	22.0	5.64
S32-C3-1	165×154×3	0.99	0.14	0	820	4.6	1507	21.8	4.74
S12-C1-2	160×154×5.5	2.17	0.14	466	1800	8.3	2911	26.6	3.20
S12-C2-2	160×154×5.5	1.93	0.14	487	2000	8.3	2921	26.1	3.14
S12-C3-2	160×154×5.5	2.12	0.14	470	1900	9.6	2997	27.8	2.91
S22-C1-2	166×154×4.4	1.38	0.14	397	1650	7.5	2488	26.8	3.57
S22-C2-2	166×154×4.4	1.23	0.14	419	1800	5.4	2531	20.5	3.80
S22-C3-2	166×154×4.4	1.35	0.14	401	1700	6.7	2496	21.3	3.18
S32-C1-2	165×154×3	1.01	0.14	342	1350	5.9	1919	20.2	3.42
S32-C2-2	165×154×3	0.90	0.14	356	1500	6.7	1827	21.2	3.16
S32-C3-2	165×154×3	0.99	0.14	344	1400	6.9	1908	22.4	3.25
S12-C1-3	160×154×5.5	2.17	0.14	933	1880	8.9	2992	27.1	3.04
S12-C2-3	160×154×5.5	1.93	0.14	975	2100	8.6	3599	28.9	3.36
S12-C3-3	160×154×5.5	2.12	0.14	940	2400	13.2	3420	31.3	2.37
S22-C1-3	166×154×4.4	1.38	0.14	795	2050	7.9	2965	23.1	2.92
S22-C2-3	166×154×4.4	1.23	0.14	838	2100	8.0	2870	20.5	2.56
S22-C3-3	166×154×4.4	1.35	0.14	802	1800	5.6	2070	18.0	3.21
S32-C1-3	165×154×3	1.01	0.14	684	1530	6.5	2135	19.7	3.03
S32-C2-3	165×154×3	0.90	0.14	711	1650	6.0	1973	20.3	3.38
S32-C3-3	165×154×3	0.99	0.14	688	1720	5.1	2076	18.1	3.55
S43-C4-1	161×600×6.5	4.06	0.5	0	1500	5.9	1830	27.0	4.58
S44-C4-1	161×800×6.5	4.06	1	0	1080	5.0	1220	12.7	2.54
S53-C4-1	165×600×4.1	2.06	0.5	0	883	3.3	1151	37.2	11.27
S54-C4-1	165×800×4.1	2.06	1	0	648	2.5	732	16.7	6.68

index, and is defined in Eq. (3).

Fig. 7 shows four groups of specimens'  $P$ - $f$  curves with different axial compression ratios ( $\mu$ ), and shows that with the increase of the axial compression ratio, the maximum bearing capacity of the

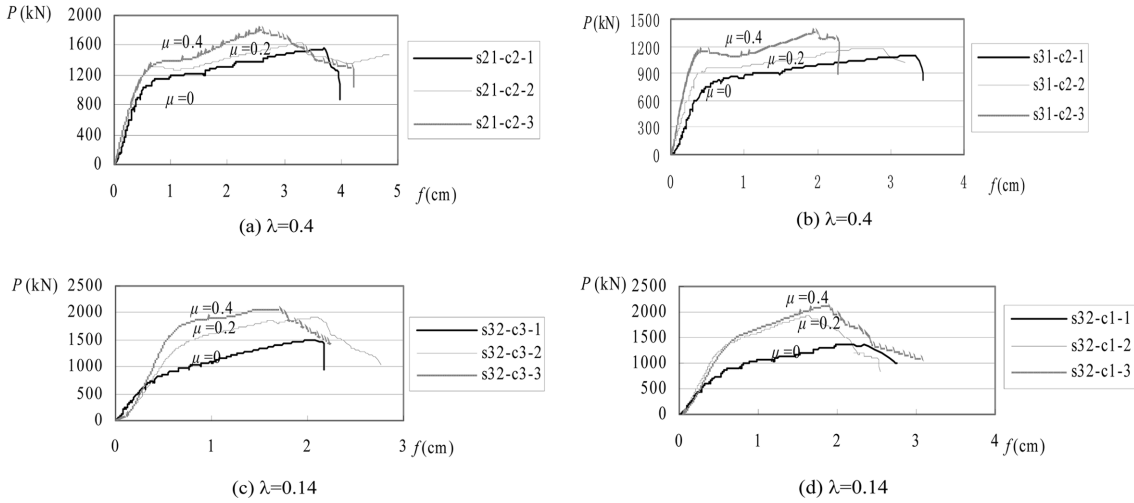


Fig. 7 Influence of axial compression ratio ( $\mu$ )

specimen ( $P_D$ ) and the capacity of linear elastic stage ( $P_A$ ) increases.

Fig. 8 shows two groups of specimens'  $P$ - $f$  curves with different shear span ratios, and shows that with the increase of the shear span ratio, the ultimate bearing capacity of the specimen ( $P_D$ ) decreases, but deflection corresponding to failure ( $f_E$ ) increases significantly. Specimens with a higher shear span ratio experienced a longer elastic-plastic stage and improved ductility.

In summary, the specimens' load-displacement curves show that CCFTs possess excellent deformation properties, good ductility and ductile failure mode under transverse shear. The measured ductility factors are shown in Fig. 9, and 90% of them are more than 3.

### 3.3 Influence of endplate

When the endplate is very close to the support, the endplate shows a very notable convex deformation through the extrusion of the internal concrete (Fig. 10). When the welded connection between the endplate and column is inadequate, the specimen may fail due to weld rupture before reaching maximum bearing capacity (Fig. 11). At first, three short specimens ("S12-C1-1", "S12-C2-1" and "S12-C3-1") failed due to weld rupture.

To solve the problem, the double welding method was used to strengthen the welds of the remaining

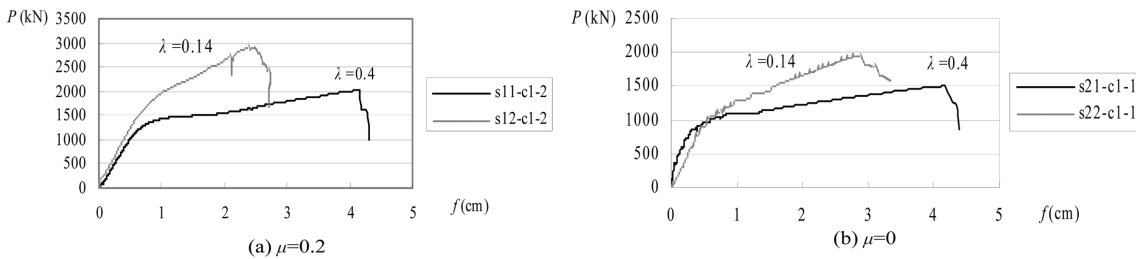


Fig. 8 Influence of shear span ratio ( $\lambda$ )

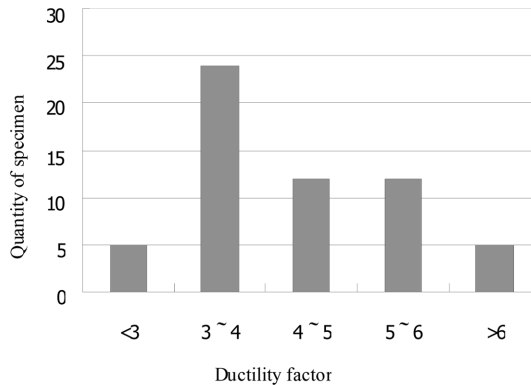


Fig. 9 Distribution of ductility factors of specimens



Fig. 10 Convex deformation of endplate



Fig. 11 Weld rupture of endplate

48 specimens. Long specimens “S11-C3-3”, “S21-C3-3”, and “S31-C3-3” were set as small shear span ratio specimens, with the new names “long to short S12-C3-1”, “long to short S22-C3-1”, and “long to short S32-C3-1”. They retained the same characteristics (including section size, material property, shear span ratio, axial compression ratio, and confinement index) as corresponding short specimens (“S12-C3-1”, “S22-C3-1” and “S32-C3-1”). “S12-C3-1” was one of the three specimens that had failed due to weld rupture.

Fig. 12 shows  $P-f$  curves for “long to short S12-C3-1” and “S12-C3-1”. Test results showed that the “long to short” specimen resulted in shear failure mode, and possessed a higher bearing capacity than the short specimen that had failed due to weld rupture.

Fig. 13 shows  $P-f$  curves for short specimens after weld strengthening and their corresponding “long to short” specimens. The figure shows that the two types of specimens have similar shear capacities. Two types of specimens had the same failure mode: rupture of the steel tube by shearing at the supports. Therefore, the double welding method was applicable.

### 3.4 Calculation of shear capacity

Due to the supporting role of core concrete on steel tubes and the confinement effect of steel tubes on core concrete, CCFTs can maintain the stability of cross sectional geometry under the transverse shear effect. Therefore, for the limit state, the ultimate shear capacities of the steel tube and core concrete can

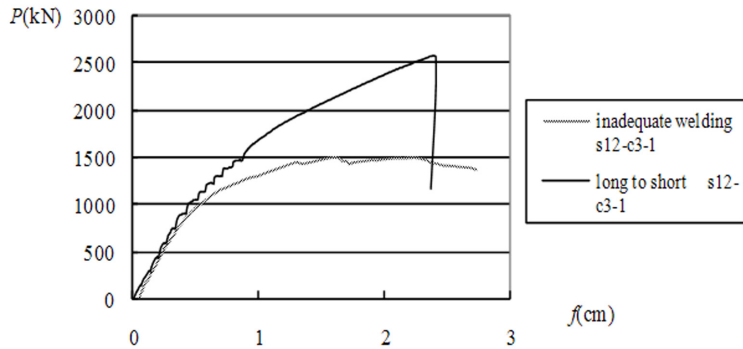


Fig. 12 Influence of inadequate welded connection

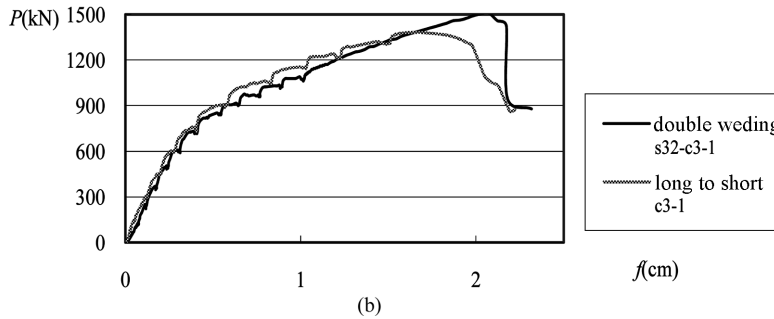
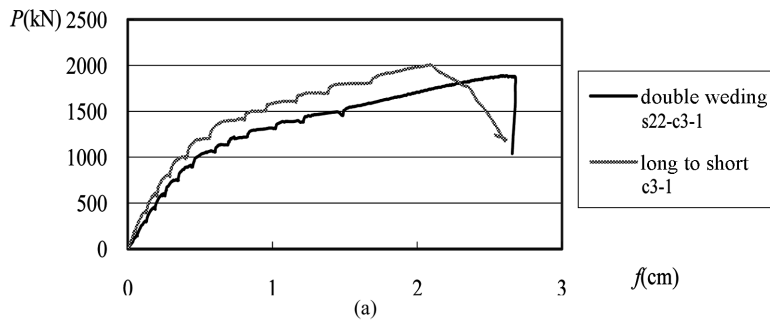


Fig. 13 Effect of weld strengthening

be added according to limit equilibrium conditions.

To simplify the formula, without regard for the confinement effect's contribution to the shear capacity of core concrete, concrete shear strength is calculated as

$$f_{cv} = 2f_t \approx 0.2f_c \tag{1}$$

Steel shear strength is calculated as

$$f_{sv} = \frac{f_s}{\sqrt{3}} \approx 0.6f_s \tag{2}$$

The “pure shear capacity” of steel tube concrete under zero shear span ratio is calculated as

$$V_0 = A_c f_{cv} + A_s f_{sv} = 2A_c f_t + 0.6A_s f_s \approx 0.2A_c f_c (1 + 3\theta) \tag{3}$$

where  $V_0$  is pure shear capacity of steel tube concrete,  $A_c$  is cross-section of core concrete,  $f_t$  is tension strength of core concrete,  $f_c$  is compression strength of core concrete,  $A_s$  is cross-section of steel tube,  $f_s$  is yield strength of steel tube, and  $\theta$  is confinement index.  $\theta$  is defined as  $\theta = f_s A_s / f_c A_c$ .

Test results showed that with the increase in shear span ratio, the shear capacity of CCFTs decreased. Fig. 14 shows the distribution of shear capacities of specimens without axial compression force. The figure shows that when the shear span ratio is no more than 2, the relationship of shear capacity ( $V_u$ ) and shear span ratio ( $\lambda$ ) can be written as

$$V_u = V_0 (1 - 0.45 \sqrt{\lambda}) \tag{4}$$

The formula is conservative and roughly the lower limit of test results (In Fig. 14, the three points below the curve represent the three short specimens which failed due to weld rupture). Cai (2003) derived the lower limit of shear capacity of CCFTs based on bending strength (see Eq. (5)) and this formula is consistent with the formula of this article at  $\lambda = 2$ .

$$V^{(-)} = 0.1N_0 \tag{5}$$

Where  $N_0$  is axial compression capacity of short CCFTs,

$$\text{when } \theta \leq 1, N_0 = A_c f_c (1 + 2\theta) \tag{6}$$

$$\text{when } \theta > 1, N_0 = A_c f_c (1 + \sqrt{\theta} + \theta) \tag{7}$$

Test results shows that, when axial compression force ( $N'$ ) exists, CCFTs experience an increase in

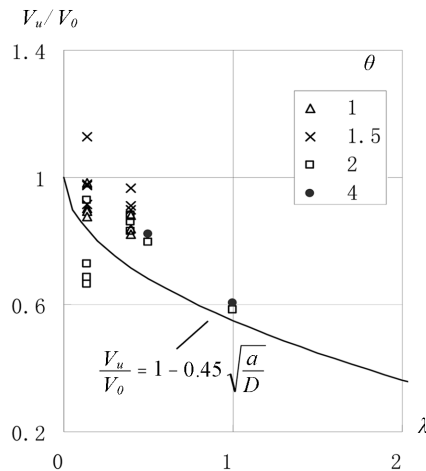


Fig. 14 Calculated shear capacities and test results for specimens without axial compression force

shear capacity, and the increase can be written as

$$\Delta V = fN' \tag{8}$$

The factor  $f$  can be referred to as the influence factor, and the measured average values of  $f$  are shown in Table 4.

Table 4 shows that with increases in the shear span ratio  $\lambda$  or axial compression ratio  $\mu$ , the value  $f$  decreases. However, factors affecting  $f$  are complex and not limited to  $\lambda$  and  $\mu$ . Conservatively using  $f=0.1$ , the shear capacity of CCFTs with the effects of shear span ratio  $\lambda$  and axial compression force  $N'$  is calculated as

$$V_u = (V_0 + 0.1N')(1 - 0.45\sqrt{\lambda}) \tag{9}$$

Fig. 15 shows a comparison of the formula and test results. The figure shows that the formula is conservative.

### 4. Conclusions

This paper mainly presents an experimental study on CCFTs under lateral load combined with axial load. The parameters of the experiment included axial compression, shear span ratio, and confinement index. Based on this study, the following conclusions can be drawn:

- CCFTs with a small shear span ratio may fail in shear in a ductile manner.

Table 4 Measured average values of  $f$

$\lambda$	$\mu$	
	0.14	0.4
0.2	0.82	0.25
0.4	0.53	0.18

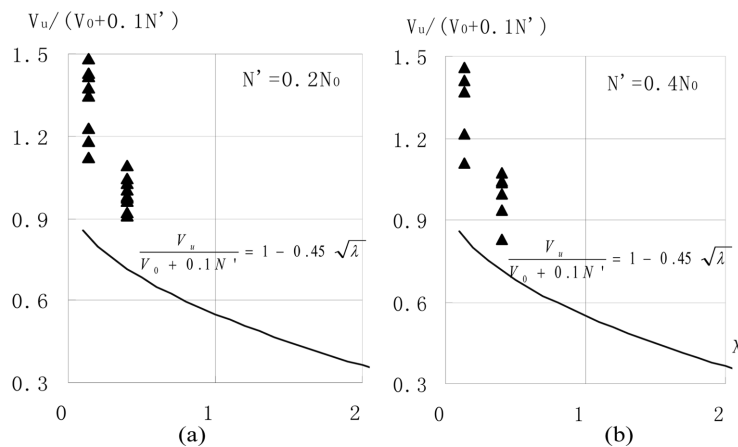


Fig. 15 Calculated shear capacities and test results for specimens with axial compression force

- A shear capacity formula for CCFTs with and without axial load is proposed. The formula is simple in form and convenient to use. It reflects the effects of several factors: size of the specimen, material properties, shear span ratio, axial compression, and confinement index.

## References

- AISC (2010), *Specification for Structural Steel Buildings*, ANSI/AISC 360-10, Chicago, IL.
- American Concrete Institute ACI. (2008), *Building code requirements for structural concrete and commentary*, Farmington Hills, Mich.
- Cai. S.-H. (2003), *Modern Concrete Filled Steel Tube Structures*, China Communications Press, Beijing, China, (in Chinese).
- Eurocode 4, European Standard (2007), *Design of composite steel and concrete structures, Part 1-1: General rules and rules for buildings*, EN 1994-2.
- Goode, C.D. (2008), "Concrete-filled steel tube columns-tests compared with Eurocode 4", *Proceedings of the sixth International Conference on Composite Construction in Steel and Concrete*, Tabernash, Colorado, July.
- Han, L.-H., Yao, G.-H. and Tao, Z.(2007), "Performance of concrete filled thin-walled steel tubes under pure torsion", *Thin-Walled Struct.*, **45**(1), 24-36.
- Han, L.-H. and Zhong, S.-T.(1992), "The Behavior Studies for CFST Shearing Problem", *J. Harbin Archit. & Civ. Eng. Inst.*, **25**(4), 32-38.
- Lee, E.T., Yun, B.H., Shim, H.J., Chang, K.H. and Lee, G.C. (2009), "Torsional Behavior of Concrete-Filled Circular Steel Tube Columns", *ASCE J. Struct. Eng.*, **135**(10), 1250-1258.
- Morino, S., Uchikoshi, M. and Yamaguchi, I. (2001), "Concrete-filled steel tube column system-its advantages", *Inter. J. Steel Struct.*, **1**(1), 33-44.
- Roeder, C.W., Cameron, B. and Brown, C.B. (1999), "Composite action in concrete filled tubes", *ASCE J. Struct. Eng.*, **125**(5), 477-784.
- Roeder, C.W., Lehman, D.E. and Thody, R. (2009), "Composite action in CFT components and connections", *AISC, Eng. J.*, **47**(4), 229-242.
- Roeder, C.W., Lehman, D.E. and Bishop, E. (2010), "Strength and stiffness of circular concrete-filled tubes", *ASCE J. Struct. Eng.*, **136**(12), 1545-1553.
- Standard of the Construction Standard Committee of China (1992), *Specification for design and construction of concrete-filled steel tubular structures (CECS 28:90)*, Planning Press, Beijing, China, (in Chinese).
- Tomii, M., Yoshimura, K. and Morishita, Y. (1977), "Experimental studies on concrete filled steel tubular columns under concentric loading", *Proceedings of International Colloquium on Stability of Structures Under Static and Dynamic Loads*, 718-741.
- Yang, W.-H. and Zhong, S.-T. (1994), "A research on the shear modulus of concrete filled steel tubes with simple beam experiments", *J. Harbin Archit. & Civ. Eng. Inst.*, **27**(6), 28-34.

UY